JOURNAL OF PROPULSION AND POWER
Vol. 14, No. 4, July–August 1998

Modeling and Estimation for Electromechanical Thrust Vector Control of Rocket Engines

Dale E. Schinstock,* Douglas A. Scott,† and Tim A. Haskew‡
University of Alabama, Tuscaloosa, Alabama 35487

Increased use of electromechanical actuators (EMA) in high-power, flight-critical applications where hydraulics have traditionally been employed has increased the need for accurate, measurable models of the EMA-load systems. Thrust vector control (TVC) of rocket engines is such an application. An intuitive, linearized model of a TVC–EMA system is presented along with practical and accurate methods of estimating the model parameters. The estimation techniques are a combination of calculations using engineering design data and of experiments based on first principles that are designed to isolate the effects of specific parameters and/or combinations of parameters. The techniques use measurements that are commonly available in an EMA system and inputs that are easily generated with either a computer or signal generator. The validity of the model and the parameter estimation techniques are experimentally verified with a pendulum simulator of a rocket engine and an EMA designed for TVC. Nonlinearities are discussed and simulated, and resonance shifting caused by backlash is demonstrated with experimental data.

Nomenclature

b_1 = equivalent translational damping of the actuator
b_2 = equivalent translational damping of the pendulum
d_{cg} = length between the pendulum's c.g. and pivot
d_1 = actuator's moment arm about the pendulum pivot
d_2 = hammer's moment arm about the pendulum pivot
F = force equivalent to the developed motor torque
F_d = equivalent disturbance force
F_h = force input from an impulse hammer
F_t = force transmitted in the spring
g = gravitational constant
I, I_c = actual and commanded motor current
J_m, J_s, J_{g1}, J_{g2} = mass moments of inertia for the motor armature, screw, gear 1, and gear 2
J_p = pendulum's moment of inertia about its pivot
k = lumped equivalent spring rate
k_b = motor back emf constant
k_f, p_f = gain and break point of the dynamic-force-feedback filter
k_p, k_i, k_d = proportion-integral-derivative position controller gains
k_{pi}, k_{ii} = proportion-integral current controller gains
k_t = motor torque constant
k_2 = pendulum's equivalent spring rate caused by gravity
L = motor inductance
l = lead of the screw
m_p = actual mass of the pendulum
m_1 = actuator's equivalent translational mass
m_2 = pendulum's equivalent translational mass
N = ratio of motor rotation to nut translation
n_1, n_2 = number of teeth on gear 1 and gear 2
R = motor resistance
T = developed torque on the motor armature
V = applied average motor voltage
x_c = commanded position
x_1 = equivalent translation of the motor rotation
x_2 = equivalent translation of the pendulum rotation
ω_n = resonant frequency of mechanical system

Introduction

FOR a variety of reasons, there is a tendency within the aerospace community to explore the use of electromechanical actuators (EMA) in applications where hydraulics have traditionally been employed. Thrust vector control (TVC) and flight-critical, control-surface actuation are examples of such applications. Advances in EMA technologies, such as permanent-magnet machines and power electronics, have made these systems a viable alternative to hydraulics in high-power applications. Potential benefits include increased reliability, reduced weight and volume of the end-to-end power and actuation system, and decreased maintenance requirements. Evidence of the shift toward EMA technology can be found in the Power-by-Wire[1] program in the U.S. Air Force and the commitment of NASA to use all electric actuation on future spacecraft.[2] The X-33 Advanced Technology Demonstrator is one such spacecraft.

Before EMA are widely accepted by the aerospace community at large for flight-critical actuation, extensive research, development, and testing must be performed. The purpose of the material presented here is to analyze the EMA–TVC system and to present simple but encompassing models along with practical methods of estimating the parameters in these models. The main purpose of the models developed here is control system design and analysis.

The insight for the model development is the result of knowledge of the significant dynamics of EMA and previously

Received Nov. 21, 1997; revision received March 6, 1998; accepted for publication March 7, 1998.

*Assistant Professor, Mechanical Engineering Department, Box 870276. E-mail: dschin@coe.eng.ua.edu.
†Research Assistant, Mechanical Engineering Department, Box 870276.
‡Associate Professor, Electrical Engineering Department, Box 870286.

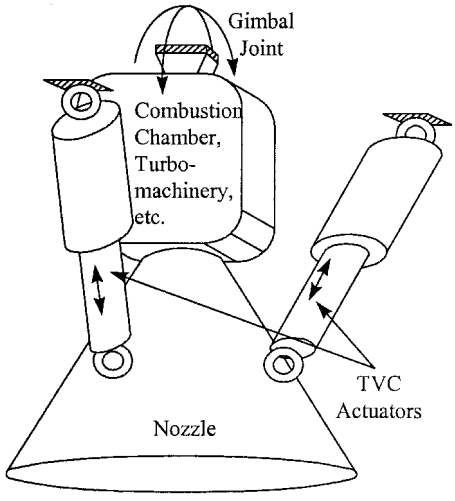

Fig. 1 Actuator placement for thrust vector control.

determined dynamics of hydraulic TVC systems.[3] The approach used for estimation of parameters is a combination of calculations using engineering design data and of experiments designed to isolate the effects of specific parameters and/or combinations of parameters. This brute-force approach to parameter estimation is in stark contrast to methods that simultaneously estimate all of the parameters of black box or ready made models.[4–8] These seemingly elegant approaches to parameter estimation suffer from many problems, including difficulties with estimation of parameters for continuous-time models.[6–10] The brute-force approach allows accurately calculated parameters to be incorporated into the model. Also, as many agree,[6–9] the estimation of continuous-time models leads to an intuitive system representation consistent with the conceptual design procedures used for most control systems, which are still based in classical theory.

TVC, as it is considered here, is the control of thrust direction from a rocket engine using linear actuators to gimbal the engine. On all spacecraft to date, these actuators have been hydraulic. In fact, EMA have never been used for TVC, even in ground testing of the engine systems. The actuator configuration for TVC is illustrated in Fig. 1. The rocket thrust is directed using two actuators. There will be some parameter variation in the linear models because of engine rotation. However, these effects are neglected because the angles are small; typically less than 10 deg. Also, because of small angles and the fact that the actuators are mounted 90 deg apart around the circumference of the engine, the coupling between the dynamics of the two actuators is neglected.

Hardware and Instrumentation

TVC simulators currently in use by the Component Development Division of the Propulsion Laboratory at NASA Marshall Space Flight Center (MSFC) utilize an actuator–pendulum configuration. These simulators have been used throughout the U.S. space program in experimentation and control system development for hydraulic TVC actuators. Mounting the actuator in series with a pendulum captures the greatest majority of the dynamics of an actuator–TVC system. All of the experimental data presented here were obtained using a TVC simulator at NASA MSFC with a 1-hp EMA designed for the RL-10 Pratt and Whitney engine. Figure 2 schematically illustrates the TVC simulator and the experimental hardware used.

The major components in the experimental hardware are a Pentium™ personal computer with an A/D interface card for data acquisition and control, pulse-width-modulated (PWM) motor controller, the 1-hp EMA actuator, and the TVC simulator. The motor controller is essentially a transimpedance amplifier, converting an input voltage to a motor current. Instrumentation includes a resolver mounted on the screw that is integral to the actuator, a load cell mounted in the tailstock of the actuator, motor current sensing in the motor controller, and a string potentiometer attached to the pendulum. In addition, a large impulse hammer with a piezoelectric load cell is used to generate a disturbance impulse force.

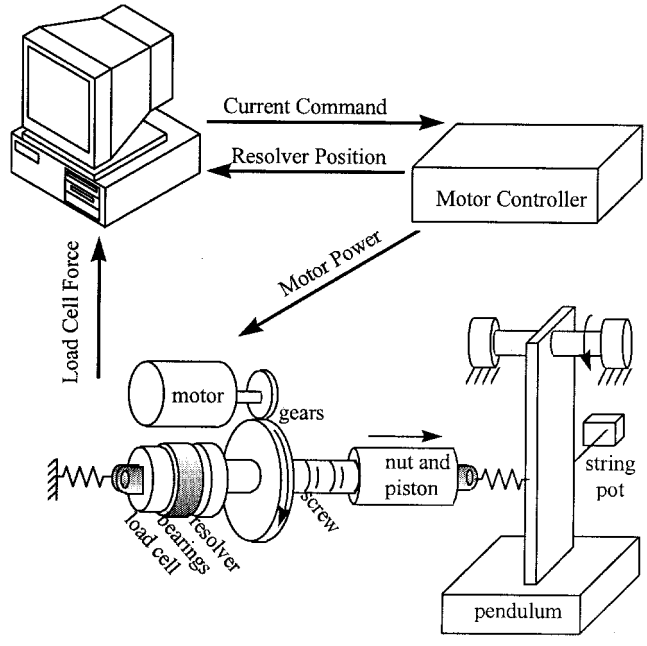

Fig. 2 Experimental hardware.

Modeling

Figure 3 gives a pictorial representation for the model development of the mechanical system. The analogous translational mechanical system is an intuitive model from which a great deal of insight can be obtained with minimal effort. It captures the dominant features of this system as well as important features of more complex aircraft and space structure vibration control problems[11] and most machine tool axes.

The modeled spring captures the major cumulative effects associated with the stiffness of actuator attachment points, the pendulum arm (or engine nozzle), torsional windup of the screw, and other actuator components. In past hydraulic–TVC systems, the major stiffness effects have been attributed to the nozzle, attachment points, and compression of the hydraulic fluid. It has been demonstrated that these effects result in fairly low resonance (as low as 8 Hz) in most hydraulic–TVC systems. The damping for this spring will be quite small because it is mainly structural damping.

The two masses, m_1 and m_2, are equivalent masses for mass moments of inertia of the rotating actuator components and the pendulum (or engine) moment of inertia, respectively. In almost all cases, the motor inertia will be the most significant because of the large mechanical advantage of the screw drive system. Inertial effects caused by translation of the entire actuator resulting from tailstock compression will be quite small because the mass of the actuator is small compared with the two equivalent masses. The two damping coefficients, b_1 and b_2, are attributed to the friction in the actuator components and the pendulum bearings (or engine gimbal). Actuator friction is large in comparison with that of the pendulum or engine.

The equivalent masses may be calculated from mass properties obtained from vendors and/or mechanical design data for the actuator and the pendulum (or engine). Reflecting the inertia for each of the rotating components in the actuator to translation of the nut results in

$$m_1 = [(J_m + J_{g1})/N^2] + (J_s + J_{g2})(2\pi/l)^2 \qquad (1)$$

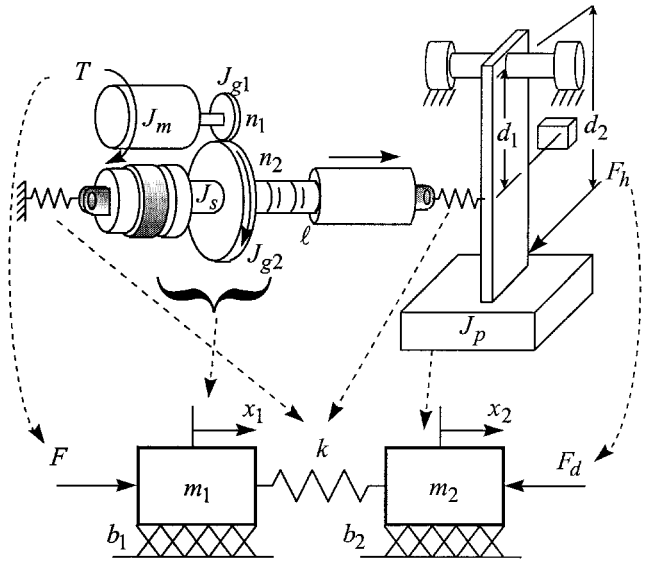

Fig. 3 Model development.

where

$$N \equiv n_1 l/(2\pi n_2) \tag{2}$$

There is no approximation involved in Eq. (1).

Applying the concept of virtual work,[12] and using a small angle approximation, the equivalent mass for the pendulum (or engine) is obtained. Ignoring the friction effects, the torque applied to the pendulum by an actuator can be equated to the inertial torque, and the power associated with this torque found

$$T_p = F_p d_1 = J_p \ddot{\theta}_p \tag{3}$$

$$\text{Power} = T_p \dot{\theta}_p = J_p \ddot{\theta}_p \dot{\theta}_p \tag{4}$$

For small angles, where the actuator is approximately perpendicular to d_1

$$\dot{\theta}_p \cong \frac{\dot{x}_2}{d_1}, \qquad \ddot{\theta}_p \cong \frac{\ddot{x}_2}{d_1} \tag{5}$$

Equations analogous to Eqs. (3) and (4) can be written assuming that the pendulum can be modeled as a translating mass

$$F_p = m_2 \ddot{x}_2 \tag{6}$$

$$\text{Power} = F_p \dot{x}_2 = m_2 \ddot{x}_2 \dot{x}_2 \tag{7}$$

Substituting Eq. (5) into Eq. (4) and equating Eqs. (4) and (7) gives

$$m_2 = J_p/d_1^2 \tag{8}$$

This result is a linearization. The same analysis can be performed for an engine except that the equivalent moment arm of the actuator would be used rather than d_1 because the actuator will, in general, not be perpendicular to the line between the gimbal and the attachment point.

Other mechanical parameters are estimated through experimentation. Parameters for the motor are determined from motor manufacturing data.

Forces in the translational mechanical model that are equivalent to the developed motor torque and impulse hammer force are given by Eqs. (9) and (10), respectively

$$F = T/N = k_t I/N \tag{9}$$

$$F_d = F_h(d_1/d_2) \tag{10}$$

The complete linear model is shown in Fig. 4. It includes the mechanical dynamics and the electrical dynamics of the brushless dc motor (BDCM). Additionally, it incorporates three separate compensation blocks: 1) A proportion-integral-derivative (PID) position controller, 2) a proportion-integral (PI) motor current controller, and 3) a dynamic-force-feedback (DFF) compensator. The position controller is implemented digitally in the computer, and the current controller is an analog controller in the transimpedance amplifier. The DFF compensation significantly reduces the effects of resonance. It also reduces the forces resulting from engine startup and shutdown transients. The DFF is implemented digitally using the load cell force measurement. The design of the compensation loops is beyond the scope of this discussion.

The electrical dynamics are not significant in the overall system dynamics because of the fast response of the current loop. The current controller was designed for a bandwidth of approximately 150 Hz.

As illustrated in Fig. 5, a nonlinear model was also developed. It incorporates several nonlinear effects: Gear backlash, screw and mount backlash, static friction, and controller output saturation.

Parameter Estimation

The coefficients of viscous friction and the spring rate are typically difficult parameters to calculate. They are therefore estimated through experimentation. The estimation methods utilize an approach in which the specific effects of coefficients are isolated in properly designed experiments.

The friction effects of a rigid-body model are determined through constant velocity experiments where the effects of inertia and spring rate are not important. Recognizing that the model in Fig. 3 is a type-1 system, with a free integrator in the transfer function relating position to the input force, one can exploit the static relationship between steady-state velocity and input torque. Using several triangular-position-profile experiments obtained from a suboptimal closed-loop system, the motor current can be determined as a function of velocity. Figure 6 shows the data from a single experiment of this type. The motor current settles to a constant value after each change in direction. The friction current, which is related to the friction torque by a constant of proportionality k_t is found by averaging the absolute values of the currents from two steady-state portions with velocities of opposite sign. This average is independent of any dc offset in the instrumentation.

Figure 7 shows the resulting motor current values obtained from many constant velocity experiments along with two separate linear fits to the data. One linear fit allows a static friction offset while the other does not. In Fig. 7 it is obvious that a viscous-friction model is not completely accurate.

One might be briefly tempted to use the load cell output rather than the motor current to determine the applied force during the constant velocity experiments. However, upon inspection of the actual hardware and the models, it should be evident that this is the force transmitted between the two masses.

A friction coefficient obtained from the procedures described earlier is that of a rigid-body model with viscous damping, $b_1 + b_2$, and a mass, $m_1 + m_2$. To obtain an estimate of how to distribute the lumped friction, the pendulum (or engine) may be modeled as a mass-spring-damper system. This linear approximation of the pendulum is governed by the following differential equation:

$$m_2 \ddot{x}_2 + b_2 \dot{x}_2 + k_2 x_2 = 0 \tag{11}$$

where

$$k_2 = m_p g d_{cg}/d_1^2 \tag{12}$$

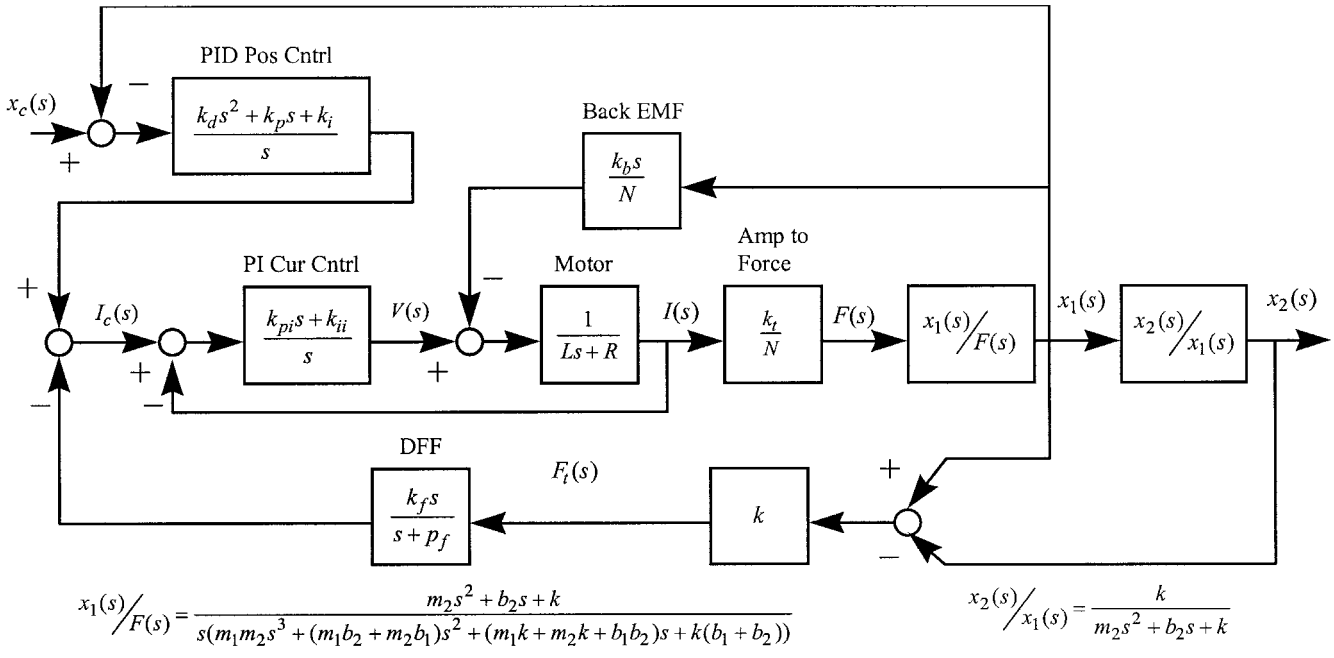

Fig. 4 Linear model.

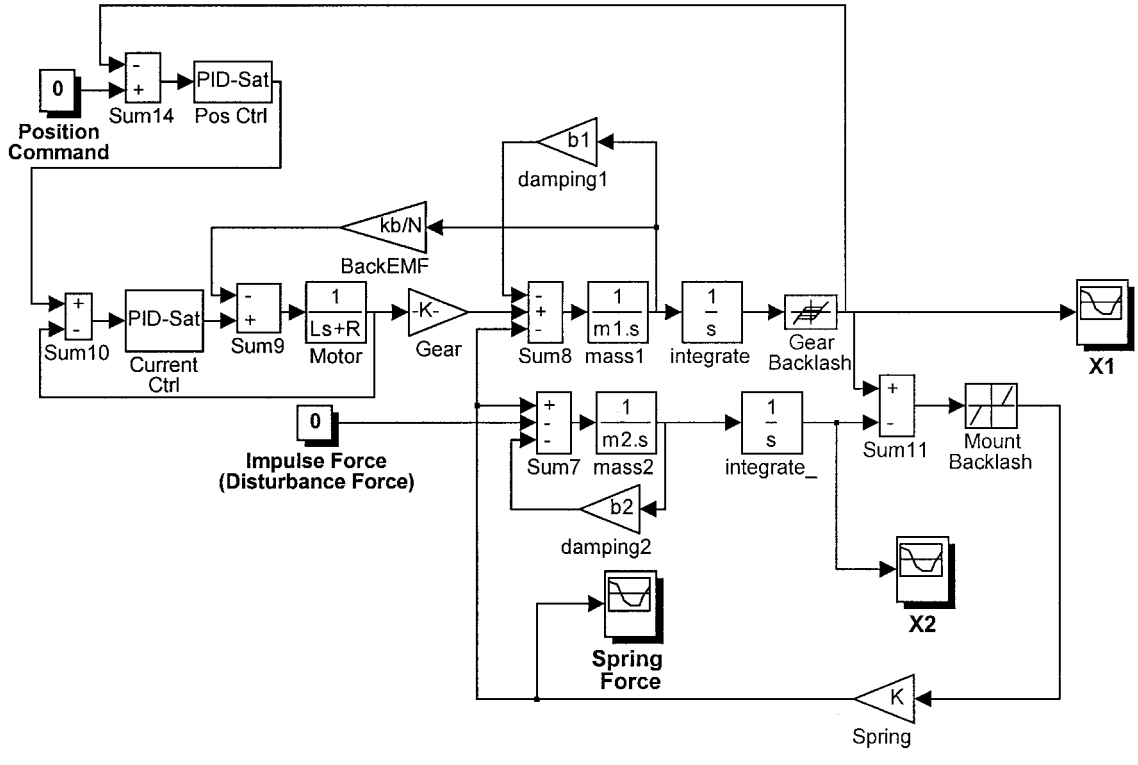

Fig. 5 Nonlinear model.

Removing the actuator and allowing the pendulum to swing freely after it is displaced results in a decaying oscillation. Using the displacement at any two successive peaks, $x_2(t_1)$ and $x_2(t_2)$, a logarithmic decrement can be calculated.[13]

$$\delta = \ell n[x_2(t_1)/x_2(t_2)] \tag{13}$$

The viscous damping coefficient can be determined from the damping ratio, ζ_p; ζ_p can be determined using the logarithmic decrement

$$b_2 = \zeta_p 2\sqrt{k_2 m_2} = (\delta/\sqrt{4\pi^2 + \delta^2})2\sqrt{k_2 m_2} \tag{14}$$

Alternatively, the distribution of the friction may be estimated by performing the constant-velocity experiments with the actuator removed from the pendulum (or engine) to obtain b_1. Or, the load cell force may be used to estimate b_2 from the constant-velocity tests with the actuator attached. Here, the logarithmic decrement solution was used for expediency because the load cell output was not available during the constant-velocity experiments. A simple educated guess at the distribution might even be sufficient for control purposes. As previously mentioned, most of the friction will be associated with the actuator mass m_1 because the friction in the pendulum bearings and/or gimbal mount of the engine will be small compared with that in the actuator.

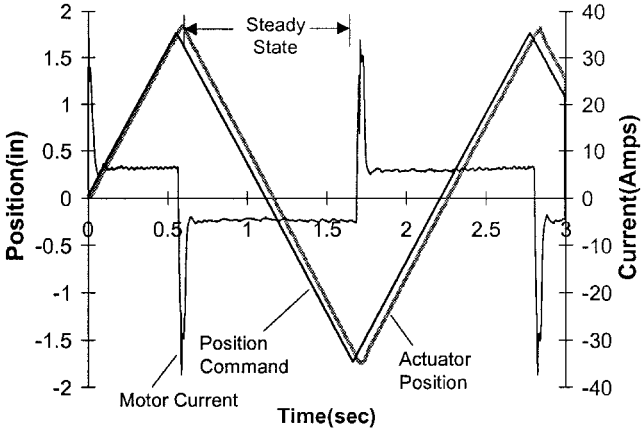

Fig. 6 Data from a single constant velocity experiment.

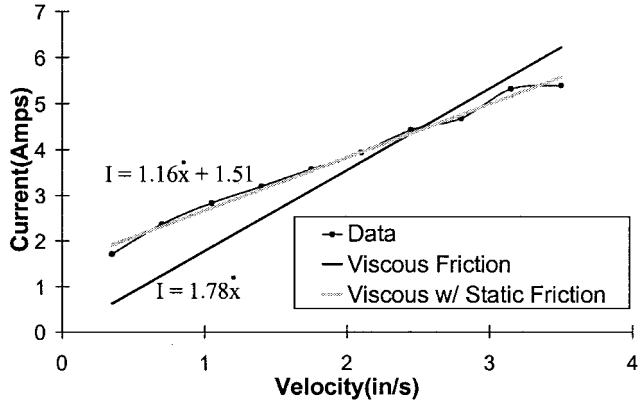

Fig. 7 Current vs velocity data from constant velocity experiments.

The methods presented for parameter estimation thus far are practical methods of determining all of the parameters for the model except the spring rate k. This parameter is perhaps the most difficult to estimate with the actuator attached to an engine. It is however, important to incorporate the dynamics contributing to resonance because it has been demonstrated to be at low frequencies in previous hydraulic systems. The resonance may be responsible for very large resultant forces on the engine and actuator during the transient portions of engine startup and shutdown.[14] Two methods of estimating k are presented here; the first of which would be difficult to perform with the actuator attached to an engine.

Bracing the pendulum with a large wooden brace between it and the test-stand structure enables estimation of the spring rate in the model. By increasing the torque in the motor slowly, the system may be loaded quasistatically while recording the load cell force, the motor position, and the pendulum position. The difference between the two positions is the compression distance of the spring. The load force is the force transmitted in the spring. The spring constant may be determined from this simple experiment. This experiment may be difficult to perform with the actuator attached to the engine because it will be difficult to fix the engine and also because an independent measure of the engine position will most likely be unavailable.

With the other parameters of the mechanical model known, the spring rate can also be estimated using the resonant frequency ω_n of the mechanical system. Resonance can easily be determined using a small-amplitude sinusoidal sweep for the current command while recording the amplitude of the load cell output. The load cell output is used because the resonant peak may be difficult to see in the motor position response and, because, as previously mentioned, an independent measure of the engine position will probably not be available.

If it is assumed that the characteristic equation for the two-mass-spring system has one real and two lightly damped complex roots, then we may factor it as follows:

$$s^3 + \frac{m_1b_2 + m_2b_1}{m_1m_2}s^2 + \frac{m_1k + m_2k + b_1b_2}{m_1m_2}s + \frac{k(b_1 + b_2)}{m_1m_2} = (s + a)(s^2 + 2\zeta\omega_n s + \omega_n^2) \tag{15}$$

If the right-hand side of Eq. (15) is expanded and the coefficients of the polynomials are equated, then ζ and a may be eliminated in developing an equation involving k as the only unknown:

$$c_1k^2 + c_2k + c_3 = 0 \tag{16}$$

where

$$c_1 \equiv \frac{(b_1 + b_2)^2}{m_1^2m_2^2\omega_n^4} \tag{17}$$

$$c_2 \equiv \frac{m_1 + m_2}{m_1m_2} - \frac{(m_1b_2 + m_2b_1)(b_1 + b_2)}{m_1^2m_2^2\omega_n^2} \tag{18}$$

$$c_3 \equiv \frac{b_1b_2}{m_1m_2} - \omega_n^2 \tag{19}$$

Although it is not proven here, the authors' experience with Eq. (16) indicates that for lightly damped systems ($\zeta < 0.3$), one of the roots of Eq. (16) can be discarded because it is negative. This equation is only intended for use with lightly damped systems, because it would be difficult to experimentally determine ω_n otherwise. It is also worth noting that in most cases, where the effective motor mass is large, k may be estimated by

$$k \cong m_2\omega_n^2 \tag{20}$$

Model Verification

The modeling and estimation methods described in the previous sections were applied to the system described by Fig. 4. The viscous damping coefficients and the spring rate were estimated from experimental data. The mass coefficients and motor coefficients were determined from manufacturer's data. The coefficients for the three compensators were determined using control design procedures. The PID-position controller was designed to provide a 5-Hz bandwidth. The coefficients of this model are given as follows:

1) Control gains: $k_p = 68.47$ A/in., $k_i = 173.43$ A/in.-s, $k_d = 4.22$ A-s/in., $k_{pi} = 0.2922$ V/A, $k_{ii} = 3.58.14$ V/A-s, $k_f = 0.9758$ A/lb, and $p_f = 1633$ l/s.

2) Motor parameters: $R = 0.38\Omega$, $L = 3.1 \times 10^4$ H, $k_t = 0.7125$ in.-lb/A, and $k_b = 0.0807$ V-s/rad.

3) Mechanical parameters: $N = 0.0062$, $m_1 = 13.8$ lb-s^2/in., $m_2 = 1.8$ lb-s^2/in., $b_1 = 144$ lb-s/in., $b_2 = 60$ lb-s/in., and $k = 4.8 \times 10^4$ lb/in.

The results shown in Fig. 8 demonstrate the validity of the linear model for control system design. This figure shows the predicted closed-loop frequency response of the linear model along with the experimentally developed response for a system without the DFF compensation. The amplitude of the sinusoidal input was 0.1 in. at all frequencies except near the resonance, where smaller amplitudes were used to prevent damage to the hardware.

In Fig. 8 there is a difference between the resonant frequencies and the amplitudes at high frequencies, where severe attenuation occurs. This can be explained by backlash in the actual system. As demonstrated in Fig. 9, which shows the experimentally measured transmitted force response caused by a hammer impulse, the frequency of oscillation is significantly

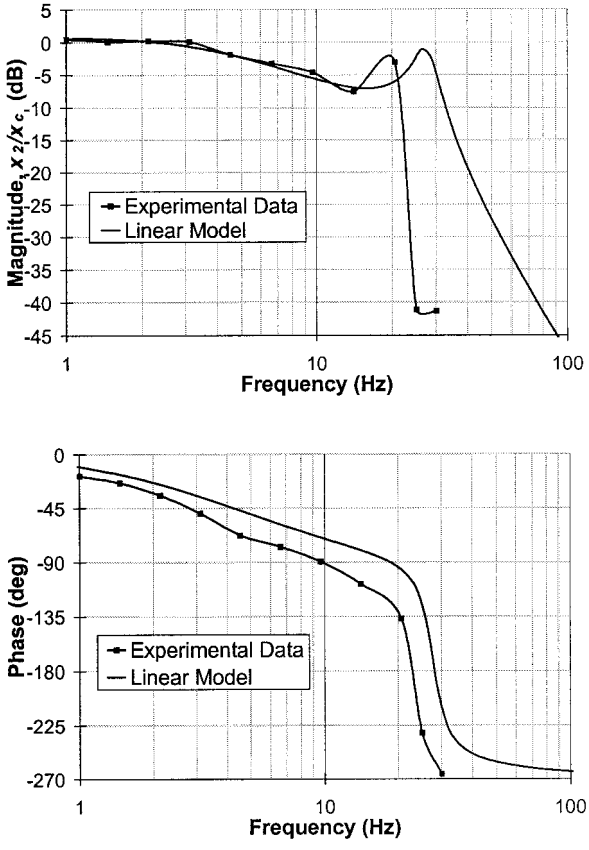

Fig. 8 Closed-loop frequency response without DFF.

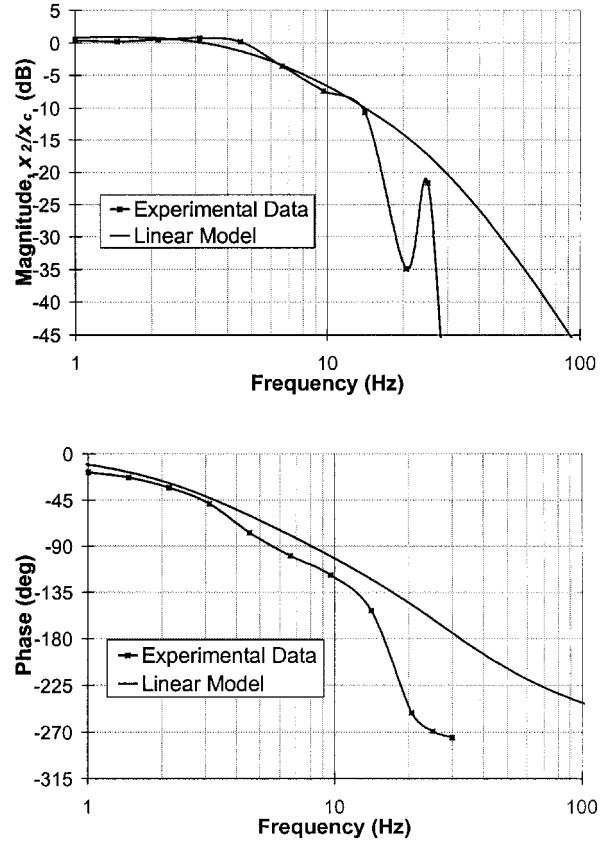

Fig. 11 Closed-loop frequency response with DFF.

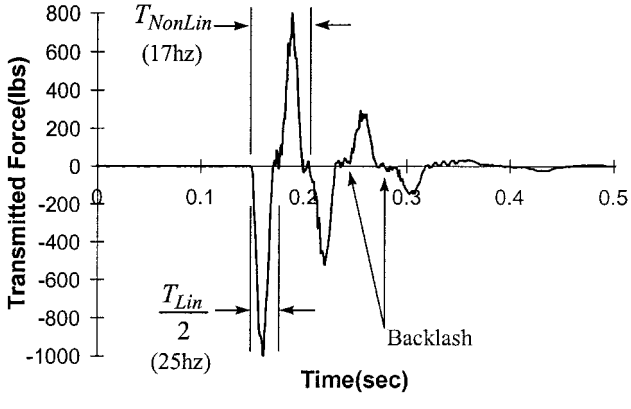

Fig. 9 Measured transmitted force because of a hammer impulse.

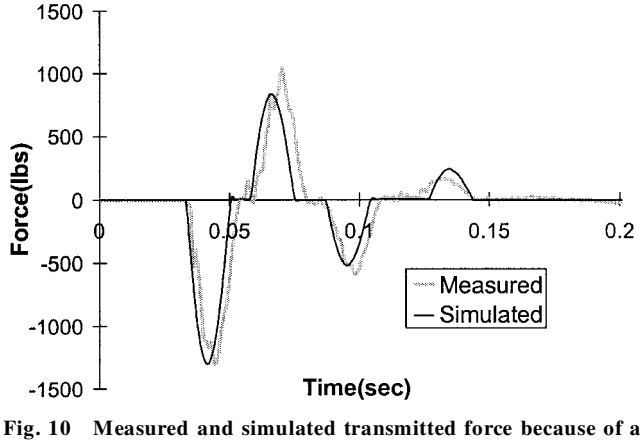

Fig. 10 Measured and simulated transmitted force because of a hammer impulse.

decreased at low amplitudes because of backlash. This frequency shift might explain the difference in the resonant frequencies for the linear model and actual system. Furthermore, the backlash also results in amplitude attenuation for small displacement values. The attenuation caused by backlash might explain the differences in high-frequency amplitude for the two plots in Fig. 8.

The effects of backlash may be captured in a nonlinear model like that in Fig. 5. Figure 10 shows the results of a simulated impulse response of the TVC–EMA system along with an experimentally measured response with the same impulse area.

The linear model may further be used to design the DFF filter to reduce the effects of resonance. The results shown in Fig. 11 demonstrate the validity of the linear model for these purposes. This figure shows the predicted closed-loop frequency response of the linear model along with the experimentally developed response for a system with the DFF compensation. The amplitude of the sinusoidal input used in the generation of Fig. 11 was 0.1 in., even near the resonance. The goal of adding the DFF compensator is to reduce the unacceptable resonant peak seen in the magnitude plot of Fig. 8. This resonance may be responsible for very large resultant forces on the actuator and engine nozzle during startup and shutdown transients of the engine. It is also undesirable from the vehicle control perspective, where the engine control dynamics are very important. Using accurate models of the higher-order dynamics in the controller design, this peak has been reduced by 20 dB (a factor of 10 for magnitude ratios) in the actual response of the system.

Conclusions

An intuitive, linearized model of a TVC–EMA system has been presented along with practical and accurate methods of estimating the model parameters. These estimation techniques

are a combination of calculations using engineering design data and experiments designed to isolate the effects of specific parameters and/or combinations of parameters. They use measurements that are commonly available in an EMA system and inputs that can easily be generated either with a computer or signal generator.

The validity of the model and the parameter-estimation techniques for classical control design has been demonstrated in an application. The experimental frequency response data for the system in the application deviates slightly from projections obtained using the linear model estimated for this system. This deviation might be explained by backlash, which cannot be included in the linear model. The nonlinear model simulations reveal that the addition of backlash increases the model accuracy. However, even with the differences between the linear model and actual system, the objectives of obtaining a model that is effective in control system design are achieved with the methods presented in the paper.

Acknowledgments

The work described here was supported in part by a NASA/American Society for Engineering Education (ASEE) Faculty Fellowship and a NASA/ASEE Accompanying Student Fellowship. It has also been supported by a NASA Grant NAG8-1407 to the University of Alabama Electromechanical Actuation Test Facility.

References

[1]Trosen, D. W., and Cannon, B. J., "Electric Actuation and Control System," *Proceedings of the 31st Intersociety Energy Conversion Engineering Conference* (Washington, DC), Vol. 1, Inst. of Electrical and Electronics Engineers, New York, 1996, pp. 197–202.

[2]Burrows, L. M., and Roth, M. E., "Electromechanical Actuation System for an Expendable Launch Vehicle," *Proceedings of the 27th Intersociety Energy Conversion Engineering Conference* (San Diego, CA), Vol. 1, Inst. of Electrical and Electronics Engineers, New York, 1992, pp. 251–255.

[3]Doane, G., and Campbell, W., "Advanced Electric Motor Flux Mapping," NAS 1.26:184317, NASA-CR-184317, NASA Marshall Space Flight Center, April 1992.

[4]Bai, E. W., "Digital Identification of a Continuous-Time System and Some Related Issues," *International Journal of Control*, Vol. 61, No. 1, 1995, pp. 149–170.

[5]Ljung, L., *System Identification, Theory for the User*, Prentice–Hall, Englewood Cliffs, NJ, 1987.

[6]Unbehauen, H., and Rao, G. P., "Continuous Time Approaches to System Identification—A Survey," *Automatica*, Vol. 26, No. 1, 1990, pp. 23–35.

[7]Young, P., "Parameter Estimation for Continuous-Time Models—A Survey," *Automatica*, Vol. 17, No. 1, 1981, pp. 23–39.

[8]Zhao, Z. Y., Sagara, S., and Wada, K., "Bias-Compensating Least Squares Method for Identification of Continuous-Time Systems from Sampled Data," *International Journal of Control*, Vol. 53, No. 2, 1991, pp. 445–446.

[9]Schinstock, D. E., and Haskew, T. A., "Identification of Continuous-Time, Linear and Nonlinear Models of an Electromechanical Actuator," *Journal of Propulsion and Power*, Vol. 13, No. 5, 1997, pp. 683–690.

[10]Sinha, N. K., "Estimation of Transfer Function of Continuous System from Sampled Data," *Proceedings of the Institution of Electrical Engineers*, Vol. 119, No. 5, 1972, pp. 612–614.

[11]Chiang, R. Y., and Safonov, M. G., "H^{∞} Robust Control Synthesis for an Undamped, Non-Colocated Spring-Mass System," *Proceedings of the American Control Conference*, 1990, pp. 966, 967.

[12]Meriam, J. L., *Engineering Mechanics*, Wiley, New York, 1992.

[13]Rao, S. S., "Free Vibration of Single Degree of Freedom Systems," *Mechanical Vibrations*, 2nd ed., Addison–Wesley, Reading, MA, 1990, pp. 63–125.

[14]Ryan, R. S., "Problems Experienced and Envisioned for Dynamical Physical Systems," NASA-TP-2508, NASA Marshall Space Flight Center, Aug. 1985.